PNAS RESEARCH ARTICLE | POPULATION BIOLOGY

Climate change could amplify weak synchrony in large marine ecosystems

Vadim A. Karatayev[a,b,c,1], Stephan B. Munch[d,e], Tanya L. Rogers[d], and Daniel C. Reuman[b,c]

Affiliations are included on p. 7.

Edited by Ottar N. Bjørnstad, The Pennsylvania State University, University Park, PA; received March 12, 2024; accepted October 27, 2024 by Editorial Board Member Pablo A. Marquet

Climate change is increasing the frequency of large-scale, extreme environmental events and flattening environmental gradients. Whether such changes will cause spatially synchronous, large-scale population declines depends on mechanisms that limit metapopulation synchrony, thereby promoting rescue effects and stability. Using long-term data and empirical dynamic models, we quantified spatial heterogeneity in density dependence, spatial heterogeneity in environmental responses, and environmental gradients to assess their role in inhibiting synchrony across 36 marine fish and invertebrate species. Overall, spatial heterogeneity in population dynamics was as important as environmental drivers in explaining population variation. This heterogeneity leads to weak synchrony in the California Current Ecosystem, where populations exhibit diverse responses to shared, large-scale environmental change. In contrast, in the Northeast U.S. Shelf Ecosystem, gradients in average environmental conditions among locations, filtered through nonlinear environmental response curves, limit synchrony. Simulations predict that environmental gradients and response diversity will continue to inhibit synchrony even if large-scale environmental extremes become common. However, if environmental gradients weaken, synchrony and periods of large-scale population decline may rise sharply among commercially important species on the Northeast Shelf. Our approach thus allows ecologists to 1) quantify how differences among local communities underpin landscape-scale resilience and 2) identify the kinds of future climatic changes most likely to amplify synchrony and erode species stability.

synchrony | environmental gradients | time-delay embedding | empirical dynamic models | spatial dynamics

Significance

Desynchronized population fluctuations promote metapopulation stability. We proposed data-driven methods to differentiate between three different synchrony-reducing mechanisms and applied them to species in two different marine ecosystems. We find that ecological dynamics vary greatly among locations, which reduces synchrony and underpins stability for many species in the California Current. In contrast, environmental gradients primarily prevent synchrony on the Northeast U.S. Shelf. Simulations show that metapopulations in both ecosystems should maintain stability as extreme environmental events increase in frequency and spatial extent. As climate change flattens environmental gradients, however, synchrony and the frequency of large-scale population crashes may increase for many species. Thus, knowing synchrony-reducing mechanisms and future environmental trends can help identify vulnerable species whose future stability might be compromised.

A striking feature in ecosystems is the tendency for populations to grow and fall in unison across large geographic areas (1). Studies utilizing long time series have revealed that ecological synchrony typically arises from synchrony in environmental conditions that drive population fluctuations (called "Moran effects"; refs. 2 and 3). Moran effects have been shown to produce widespread synchrony in a diverse array of taxa (4–6) and are increasing with climate change in several systems (reviewed in ref. 7). Importantly, synchrony can delay or prevent metapopulation recovery when periods of low abundance coincide across locations, leaving few abundant populations to seed overall recovery through rescue effects (8–10). In this sense, mechanisms that inhibit synchrony contribute to resilience and stability of spatially extended systems.

In most metapopulations, synchrony remains limited in strength, routinely being far lower than synchrony in putative environmental drivers (e.g., refs. 11 and 12); reviewed in ref. 13). Here, we identify three mechanisms that can inhibit Moran effects and ask whether they will persist under climate change. The first is *demographic response diversity*, in which populations grow differently in response to local abundance (Fig. 1*A*; we abbreviate response diversity with RD). For example, populations without Allee effects may recover from a heat wave faster. Although spatial variation in traits underlying demographic processes is ubiquitous [e.g., heterogeneity in lifespan (14) or growth rate (15)], demographic RD has been quantified only in a handful of taxa (e.g., ref. 1), most frequently as variation in carrying capacity. The second mechanism is *environmental response diversity*, in which populations differ in their response to environmental conditions (Fig. 1*B*). A heat wave, for instance, more severely impacts populations that lack thermal refugia or local adaptation to high temperatures. Although environmental RD appears widespread (e.g., refs. 16 and 17), few studies quantify its emergent impacts on spatial population dynamics and synchrony. The third mechanism is *environmental gradients*, i.e., differences in mean environmental conditions among populations. If the population response to environment is unimodal and an environmental gradient is present, synchronous changes in the environment can generate opposing responses in different populations even if there is no environmental RD (Fig. 1*C*).

This article is a PNAS Direct Submission O.N.B. is a guest editor invited by the Editorial Board.

[1]To whom correspondence may be addressed. Email: vadimk@umd.edu.

This article contains supporting information online at https://www.pnas.org/lookup/suppl/doi:10.1073/pnas.2404155121/-/DCSupplemental.

Published December 30, 2024.

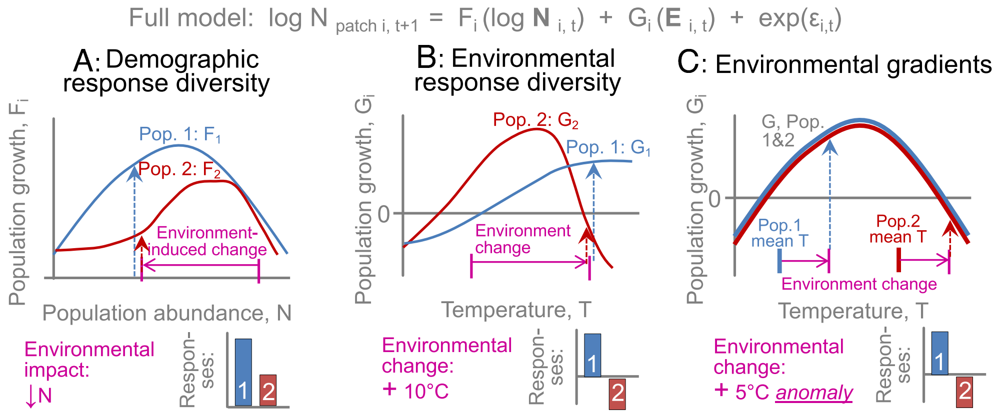

Fig. 1. Three mechanisms may explain why metapopulation synchrony is far lower than synchrony in environmental drivers. (*A*) Demographic RD through spatial heterogeneity in density dependence F_i can cause population-specific responses to an environmentally driven decline in population density (pink arrow); here, population 2 recovers more slowly. (*B*) Environmental RD through spatial heterogeneity in environment dependence G_i can cause the impacts of environmental change to differ qualitatively between populations; here, population 2 is negatively impacted due to lacking access to thermal refugia. (*C*) Gradients in mean local environment and nonlinear responses to environment (here, a unimodal thermal response curve) can also create population-specific responses: Here, a +5 °C anomaly benefits population 1, which experiences lower average temperatures, but exceeds thermal tolerances in population 2, which experiences higher average temperatures.

For instance, a +5 °C temperature change might cause mortality in equatorial populations by exceeding thermal tolerances, while benefiting poleward populations. However, the roles of RD and environmental gradients in population dynamics have not been quantified and the mechanisms mediating population synchrony in the field remain largely unknown.

Critically, the dominant mechanism can determine how a species responds to climate change. In systems where environmental gradients inhibit Moran effects, ecological synchrony and large-scale population declines may rise as climate change flattens those gradients. Temperature gradients, for instance, are flattening globally as northern latitudes (18) and higher elevations (19) warm faster than southern latitudes and lower elevations, respectively. Moreover, population synchrony may increase due to the growing frequency of extreme environmental events (20–23). This may occur either because extreme events span large areas, in effect increasing environmental synchrony, or because populations decline more strongly under severe conditions, in effect overwhelming RD. Thus, anticipating climate change impacts on synchrony requires a shift in research, from describing synchrony *patterns*, toward a data-driven understanding of synchrony *mechanisms* and how they shape spatial population dynamics.

If we had a well-vetted, data-driven, spatial population model, we could evaluate demographic RD as heterogeneity in density dependence across populations, environmental RD as heterogeneity in environment dependence, and ask whether populations respond nonlinearly to environmental drivers with gradients (Fig. 1). Unfortunately, experimentally resolving how dynamics vary across populations is not feasible in most systems. Fortunately, empirical dynamic models (EDMs) can infer population dynamics from time series without specifying the underlying equations a priori. Here, we resolve how population dynamics vary among populations by combining spatially hierarchical EDMs with survey data from two large marine ecosystems: the California Current and the Northeast U.S. Continental Shelf ("CA Current" and "NE Shelf" hereafter; Fig. 2*A* and *SI Appendix*, Table S1). For this, we compiled data spanning 40 to 48 y, 800 to 1,000 km of coastline, 11 putative environmental drivers, and 36 fish and invertebrate species. While many of these species currently have low synchrony (Fig. 2*B*), whether this stability will continue is unknown as both systems face large climatic changes (20, 24, 25).

Here, we show that spatial EDMs effectively predict observed synchrony and variation in population abundance. Next, by removing (or allowing) spatial differences in demographic RD and/or environmental RD and by removing (or allowing) environmental gradients, we quantify how each mechanism reduces metapopulation synchrony and contributes to model fit in each species. We specifically compare six nested model formulations: S_{DEG} (all three mechanisms present); S_{Deg} (demographic RD only); S_{dEg} (environmental RD only); S_{deG} (gradients only); S_{deg} (no mechanisms present); and S_{d--} (no environmental drivers and no demographic RD). Simulating the best-fitting models under altered environmental scenarios, we then show that potential climate change can alter synchrony, and therefore stability, on large spatial scales, in distinct but predictable ways depending on the aspect of climate change that one considers.

Results

We first evaluate the relevance of environmental drivers and RD in general for predicting population dynamics. Unsurprisingly, the environment has a large influence: including environmental predictors increases out-of-sample $-R^2$ (average leave-one-out R^2 value across species) from 0.21 in models with density dependence only (S_{d--}) to 0.37 (S_{deG}; Fig. 3*B*). Relevant drivers were chosen for each species via model selection: at least one ocean climate index was selected for all species, and temperature, upwelling, and/or zooplankton were also selected for 78% of species (*SI Appendix*, Table S2). Although not a physical driver, we used zooplankton as a likely proxy of local environmental productivity (26). We note that our models allow interactions between environmental drivers; preliminary models that allowed interactions between density and environment did not improve fit, and we thus model density- and environment- dependence additively (Fig. 1).

Response diversity (RD) appears as important as environment for predicting population dynamics (Fig. 3*B*): allowing for demographic and environmental RD in addition to environmental drivers further increases $-R^2$ to 0.49 (S_{DEG}; Fig. 3*B*). For several species, drivers such as ocean climate have different effects in different populations (e.g., Fig. 3 *C* and *D*). Note that this is likely an underestimate of the importance of RD, as data selection for the NE Shelf species intentionally omitted populations with qualitatively different dynamics, usually located at range boundaries (*SI Appendix*, Fig. S1 and *Methods*), often characterized by steady declines or increases that may reflect ongoing range shifts (27). Critically, our full models incorporating all synchrony-reducing

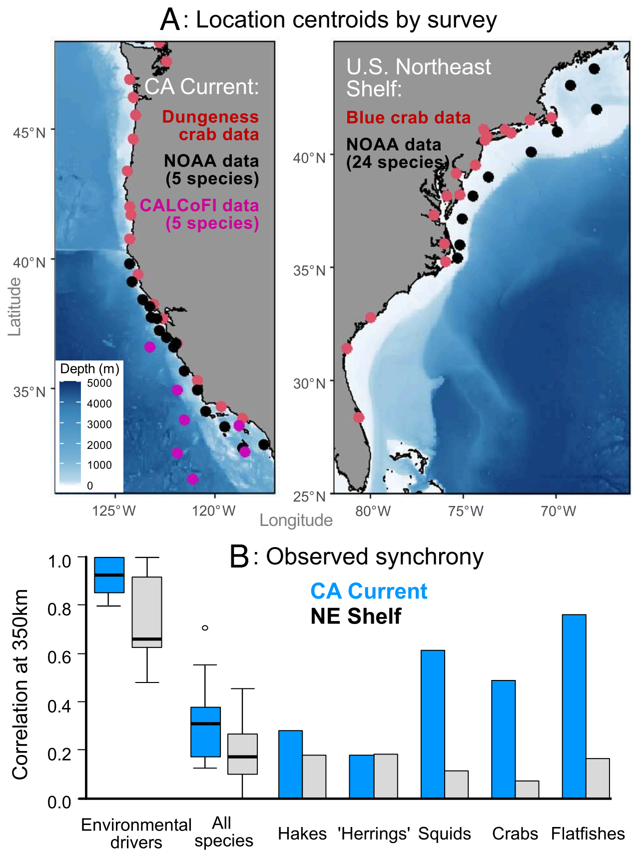

Fig. 2. Population synchrony is much lower than synchrony in environmental drivers across 36 species in two large marine ecosystems. (*A*) Study regions and centroids of locations by which survey data were aggregated; for Dungeness crab, points are port locations. (*B*) Average observed synchrony (defined as correlation at 350 km) for environmental drivers and species populations; we show synchrony for all species and for subsets of taxonomically related species that occur in both systems (Herrings denote Clupeiformes; see *SI Appendix*, Table S2 for a list of species in each subset). Synchrony is evaluated for the environmental drivers included in the best-fitting models for each species (*SI Appendix*, Table S2).

mechanisms (S_{DEG}) explain nearly half of the variation in population dynamics on average and attain a level of model-predicted synchrony close to that of data (0.35 predicted vs. 0.26 observed, medians across species).

We next compare how each of the three potential mechanisms explains dynamics and reduces Moran effects (Fig. 4 *A* and *B*). Specifically, we quantify how scenarios with demographic RD (S_{Deg}), environmental RD (S_{dEg}), gradients (S_{deG}), and all three mechanisms (S_{DEG}) increase model fit and reduce model-predicted synchrony compared to a baseline scenario with no mechanisms present (S_{deg}). We remove environmental gradients by subtracting the local mean from environmental data in each location, and then refitting and iterating models on these environmental data without gradients (see *Methods* and *SI Appendix*, Appendix D for details).

Environmental RD primarily reduces synchrony in California, while environmental gradients primarily reduce synchrony on the NE Shelf (Fig. 4*A*). Accordingly, these mechanisms play a large role in improving model fit in their respective regions (Fig. 4*B*). Environmental gradients in California and demographic RD on the NE Shelf play secondary roles in improving model fit and reducing synchrony. We also find that when mechanisms co-occur, they reduce synchrony subadditively. In 12 out of 36 species, we detected multiple mechanisms that each reduced synchrony by >0.1 when modeled individually (*SI Appendix*, Table S2). Across these 12 species, median predicted synchrony was 0.85 in models with no mechanisms, 0.32 in models with a single mechanism, and 0.28 in models with multiple mechanisms. In other words, the presence of a single mechanism reduces synchrony nearly as much as the presence of multiple mechanisms.

The fact that gradients are stronger overall on the NE Shelf than in California (Fig. 3*A*) potentially explains their greater influence in this ecosystem. However, gradient strength depends not only on system but also on which set of environmental drivers primarily influence a particular species (as determined by model selection; *SI Appendix*, Table S2). Across species, stronger gradients are associated with reduced synchrony (Fig. 4*C*, R^2 = 0.27, *P* = 0.004), although the slope of this relation is significantly negative only for gradient magnitudes <12%.

We explore three ways in which climate change might affect synchrony and the frequency of large-scale population declines. One pathway is extreme environmental events (28, 29): If synchronous drivers strongly impact organisms, they may overwhelm existing mechanisms that prevent synchrony. An intense heat wave, for instance, may exceed thermal thresholds in populations both with and without refugia from heat. Second, climate change may erode synchrony-reducing mechanisms themselves, for instance, if the loss of local adaptation to rapidly changing conditions reduces RD. A

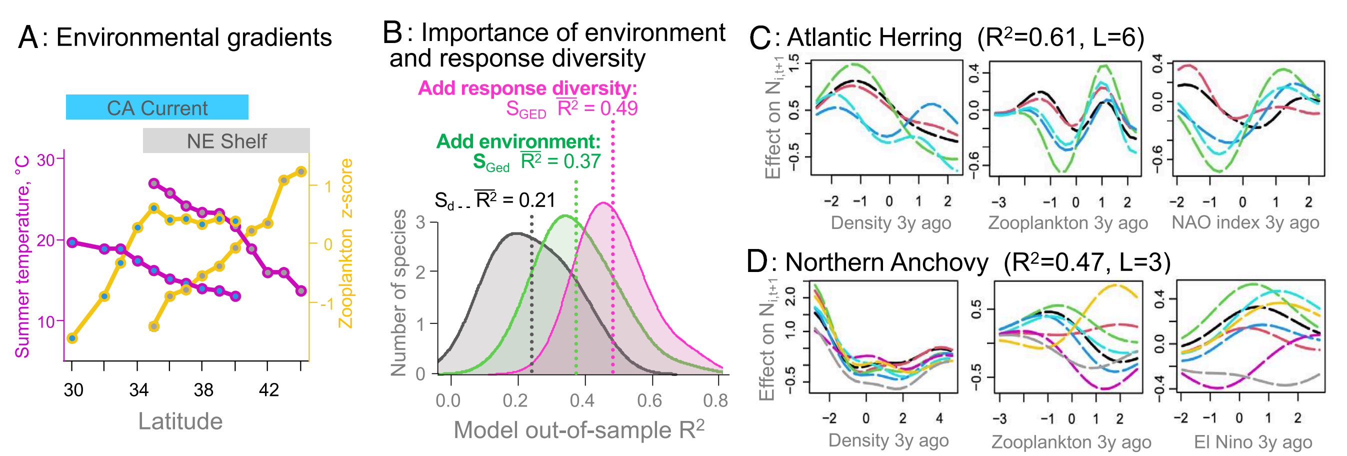

Fig. 3. Both ecosystems exhibit strong environmental gradients and demographic and environmental RD. (*A*) Latitudinal trends in mean environmental conditions in each ecosystem. (*B*) Performance of models incorporating no environmental drivers or RD (black, scenario $S_{d..}$), environmental drivers and no RD (green, scenario S_{Ged}), or both environmental drivers and RD to demography and environment (pink, scenario S_{GED}). Curves are distributions of model R^2 across 36 species; dotted lines and – R^2 values denote the means of each distribution. (*C* and *D*) Examples of RD to three drivers in models of two species, with different lines corresponding to different populations.

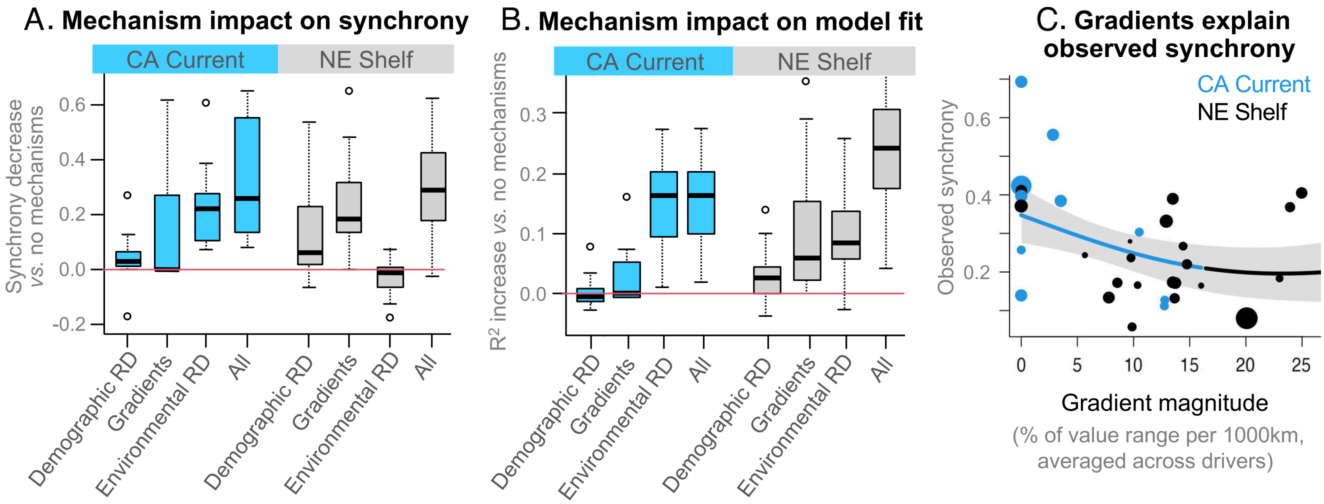

Fig. 4. Environmental RD in California and environmental gradients in the NE Shelf are the primary mechanisms that reduce synchrony, and gradient magnitude explains synchrony differences among taxa. (*A* and *B*) Decrease in predicted synchrony and increase in model fit when different synchrony-reducing mechanisms are incorporated (Demographic RD = S_{Deg}, Gradients = S_{deG}, Environmental RD = S_{dEg}, All = S_{DEG}) relative to a model with no mechanisms present (S_{deg}; see *SI Appendix*, Appendix D for model details). Bars show median and distribution of values across 36 species in California (blue) and the NE Shelf (gray). (*C*) Relationship between observed synchrony and environmental gradient magnitude (averaged across environmental predictors selected for each species). Line is a best-fit spline across species, with blue (black) portions denoting a slope found to be significantly (not significantly) different from zero and the gray area denoting 95% CI of the mean. Larger points in (*C*) correspond to species with larger geographic extent and for which gradient magnitude is better resolved.

third pathway is weakening latitudinal temperature gradients (18), which is also flattening gradients in zooplankton (24, 30) as warming, stratification, and declines in epilimnion nutrients are disproportionately greater in northern latitudes (18, 31). To evaluate these possible pathways, we simulate our best-fit models under i) an increase in extreme event frequency and spatial extent that reflects predicted increases in heat waves, mean temperature, and ocean climate variability (*Methods*), ii) a loss of response diversity, and iii) a loss of environmental gradients.

In both regions, we find that existing mechanisms can prevent high metapopulation synchrony even when environmental extremes become more common (Fig. 5*A*). By contrast, and regardless of extreme event frequency, synchrony in both regions strongly increases with the loss of gradients or RD. Greater synchrony in turn corresponds to lower stability and more frequent periods of low projected region-wide density (measured as the 10th quantile of regional density; Fig. 5*B*). The largest increases in synchrony and declines in stability arise when more frequent extreme events coincide with the loss of gradients (Fig. 5 *C* and *D*). This effect is greater in species influenced by larger gradients, highlighting how climate change impacts may vary by species. In all treatments, we find little to no change in mean population density (*SI Appendix*, Fig. S4*C*), meaning that more frequent large-scale declines arise from a loss of metapopulation stability.

Discussion

We quantify the relative importance of mechanisms that reduce population synchrony relative to the synchrony of environmental drivers, and hence promote stability, across taxa in two marine systems. Our results reveal that environmental RD and environmental gradients can greatly reduce population synchrony. The primacy of these mechanisms varied by region, reflecting the stronger gradients present on the NE Shelf, but also depended on taxa. For instance, the reduction of synchrony by gradients previously found for Atlantic blue crabs (13) occurs in a variety of other species and depends on the extent to which environmental drivers with gradients impact a species' dynamics. This variation also explains observed synchrony differences across taxa (Fig. 2*B*).

More frequent, larger-scale extreme environmental events by themselves are unlikely to impact species' regional stability (Fig. 5). Instead, synchrony and the frequency of large-scale declines will increase if climate change erodes environmental gradients or RD. This risk varies across species (Fig. 5*D* and *SI Appendix*, Table S2), underscoring previous findings that system-wide climate changes can have species-specific impacts (27). We also point out that the impacts of increased synchrony within our study species may cascade to higher trophic levels as mobile predators and fisheries cannot compensate for periods of resource depletion by moving to alternate locations (i.e., a loss of spatial portfolio effects). Altogether, our results demonstrate that without an understanding of spatial population dynamics, projections of environmental change alone tell us little about the stability of species and natural resources.

Our general results support findings of species-specific terrestrial studies. For gradients, Hagen et al. (32) found reduced synchrony across elevational temperature gradients in a moth metapopulation driven by regional climate. This indicates that our results for latitudinal gradients can also explain low synchrony at finer spatial scales. Previous studies that quantified demographic RD as spatial variation in intrinsic population growth and carrying capacity (12, 33, 34) also found that demographic RD has a limited impact on metapopulation synchrony. Simultaneously, metapopulation synchrony in these studies was low and similar to synchrony in our systems [e.g., mean correlation at 300 km = 0.30 in our study; 0.27 for six insect species in ref. 12; 0.25 for blue and great tits (34); 0.03 for cormorants (33)]. We therefore suggest that environmental gradients and environmental RD might inhibit synchrony in these other systems.

Several strategic management insights also come from our results. First, we find that temperature affects the dynamics of only a fraction of species (33%), while local productivity (zooplankton) was a more ubiquitous predictor (80% of species). This highlights that warming may primarily impact fisheries only through its potential indirect effects on productivity. Second, in our simulations, extreme events increase synchrony primarily by spanning large areas (i.e., by increasing environmental synchrony) rather than by making historically rare, extreme conditions more frequent (*SI Appendix*, Fig. S4). Both results are in line with recent work showing that population die-offs in response to marine heat waves currently appear rare

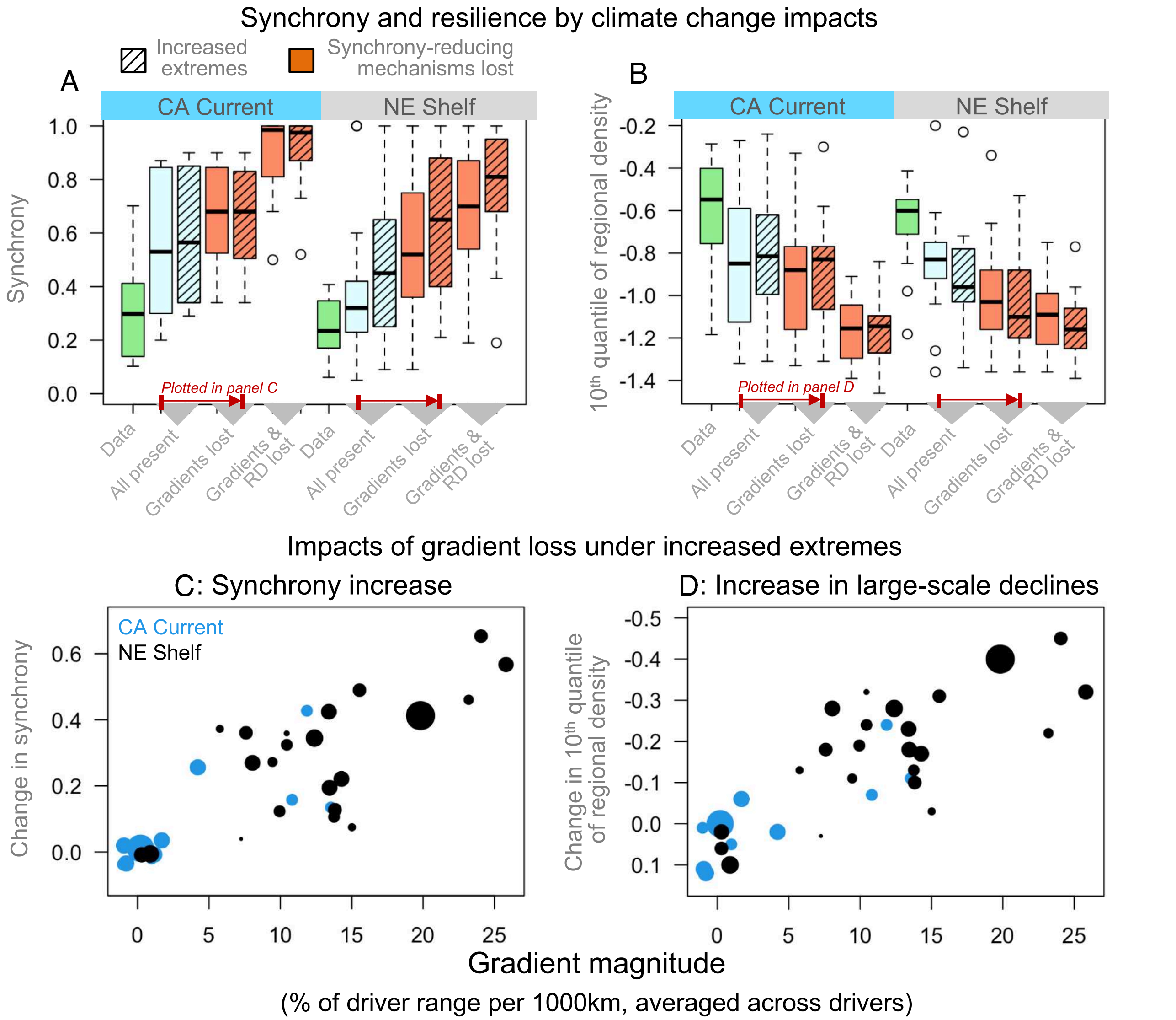

Fig. 5. Climate change is likely to increase synchrony and large-scale population declines by eroding synchrony-reducing mechanisms rather than by increasing extreme environmental events. (*A* and *B*) In EDM projections across 36 species, synchrony and large-scale declines increase to a greater extent when synchrony-reducing mechanisms are lost (orange bars) than when environmental extremes increase in frequency and spatial extent (hashed bars). Green bars are values for observed data. (*C* and *D*) Change in projected synchrony and large-scale declines with increased extremes and the loss of gradients. Points are plotted vs. environmental gradient magnitude; larger points correspond to species with larger geographic extent. 'Gradients and RD lost' simulations in *A* and *B* are projections of models without RD (scenarios S_{deG}); all other results are projections of the full models (scenarios S_{GED}).

globally (35). Third, we identified 24 species that have no or only one synchrony-reducing mechanism (*SI Appendix*, Table S2) and, in turn, may be vulnerable to increased metapopulation-wide declines. In limited preliminary analyses, we did not find a relation between the number of mechanisms and species taxonomy.

Low demographic RD and high environmental RD (Fig. 4*B*) also suggest steps for improving population models used in fisheries management. Whether and how to model spatial variation in population dynamics is a common source of debate in stock assessment models. Our results suggest that for many species, demographic processes may be similar across large areas, but there may be local differences in responses to the environment. Future assessments can readily quantify the importance of demographic and environmental RD using EDM, while fundamental research could disentangle whether environmental RD arises from heterogeneity in habitat, community composition, or local adaptation.

Several factors may affect our results. First, observation error could bias estimates of synchrony and, potentially, estimates of demographic RD. Future work could account for this using new state-space EDM methods that account for observation error (36). Observation error may explain why observed synchrony is less than predicted synchrony, although our methods account for variability in sample timing (*SI Appendix*, Appendix A). Second, a portion of the observed synchrony may be caused by mobile predators or dispersal. As EDM implicitly accounts for dispersal via time lags, our simulations are therefore unable to account for changes in mobile predators and dispersal. We note that dispersal in marine systems typically happens in early (larval) life stages, and the effect of larval supply on adult biomass is often weak. In line with this, spatial extensions of EDM found little impact of dispersal on dynamics in the NE Shelf (37). Third, our analysis may underestimate the role of gradients in reducing synchrony because spatially uniform ocean climate indices were often selected as important predictors. While climate indices themselves lack a gradient, they represent a collection of spatially heterogeneous processes such as nutrient transport and productivity. Future analyses incorporating a larger collection of spatially resolved predictors may refine our results and help resolve mechanisms.

While climate change is unlikely to eliminate RD or gradients entirely, as simulated, our study provides bounds on possible scenarios. As climate change impacts on individuals and the environment become better resolved, simulations under more realistic environmental projections could be used to identify vulnerable species whose future stability might be compromised. Improved model fits and predictions for individual species might also be attained using more species-tailored environmental drivers. Although our dataset has insufficient sample size to draw conclusions about patterns in individual taxa, differences in synchrony-reducing mechanisms across different taxonomic groups could also be explored in future work.

Unifying Population and Landscape Dynamics. Our approach advances mechanism-focused synchrony research by quantifying multiple synchrony-reducing mechanisms and how they act in concert. Critically, our nonparametric approach does not assume a parametric model (e.g., logistic dynamics) or a specific (and often unknown) population response to environment. We demonstrate that ecological dynamics vary greatly across populations and that the resulting response diversity underpins landscape stability. As such, this work complements experimental approaches that quantify resilience at the scale of individuals (e.g., thermal tolerance thresholds) but is rarely feasible at metapopulation scales.

More generally, our approach pairing long-term data with hierarchical EDMs can detect how nonlinear species' density dependence, responses to environment, and species interactions differ among local communities. Thus, future studies applying hierarchical EDMs to long-term data can directly quantify how ecological interactions and population dynamics depend on local environment and community composition. Finally, classical views contend that while "black-box" models excel at prediction, parametric models are the principal path to inferring mechanisms. Although it is true that EDM can outperform parametric models in forecasting (38), our study is one of many recent demonstrations (13, 39, 40) that appropriately constrained phenomenological models can reveal ecological mechanisms. We suggest that EDMs form a key link in scaling up our understanding from simple models to large and complex ecosystems.

Methods

Long-Term Data. We developed an annual dataset of 36 marine fish and invertebrate species by combining data from several spatially extensive, long-term surveys (*SI Appendix*, Table S1). These "species" included three larger taxonomic groups (shrimp, krill, and pelagic juvenile rockfishes). For most species, data spanned at least 10 degrees of latitude and were aggregated into one degree latitude bins ("locations" or "populations" throughout, Fig. 2*A*). Density data were log-transformed and normalized within locations. We combined biological survey data with data on 11 candidate environmental drivers (listed in *SI Appendix*, Table S2), which included winter and summer sea surface temperatures, zooplankton biomass, upwelling, and ocean climate indices. See *SI Appendix*, Appendix A for more details on data sources and data processing.

EDM Model Framework. To model population dynamics, we predict abundance changes based on past changes that occurred when the system was in a similar state. This approach effectively "reconstructs" population dynamics from time series (41) and works for nonautonomous systems with long-term change (42). In particular, we model log abundance of population i in year t, $X_{i,t}$, using the vector of lagged log population densities at times $t-L$ to $t-1$, $\boldsymbol{X}_{i,t} = \left\{X_{i,t-1,...}X_{i,t-L}\right\}$ and the vector of p different environmental drivers $\boldsymbol{E}_{i,t} = \left\{E^{1}_{i,t-1}, \cdots E^{1}_{i,t-L}, \cdots, E^{p}_{i,t-1}, \cdots, E^{p}_{i,t-L}\right\}$. We model dynamics as an additive combination of density dependence $F_i\left(\boldsymbol{X}_{i,t}\right)$ and environment-dependence $G_i(\boldsymbol{E}_{i,t})$, such that $X_{i,t} = F_i\left(\boldsymbol{X}_{i,t}\right) + G_i(\boldsymbol{E}_{i,t})$. This allows us to separately resolve demographic RD (spatial heterogeneity in F_i) and environmental RD (heterogeneity in G_i).

For each species, we fit models in two stages. We first fit a model with lags of density, $X_{i,t} = F_i\left(\boldsymbol{X}_{i,t}\right)$and computed the out-of-sample residuals $x_{i,t} = X_{i,t} - \widehat{F}_i(\boldsymbol{X}_{i,t})$, where $\widehat{F}_i(\boldsymbol{X}_{i,t})$ is the map constructed by leaving out the $(i,t)^{th}$ observation. We then fit a model to the residuals using lags of the environment, $x_{i,t} = G_i\left(\boldsymbol{E}_{i,t}\right)$. Importantly, reversing the fitting order [i.e., fitting $G_i(\boldsymbol{E}_{i,t})$ and then $F_i\left(\boldsymbol{X}_{i,t}\right)$] does not affect our qualitative results (*SI Appendix*, Appendix D). Out of sample predictions for the full model were then $\widehat{X}_{i,t} = \widehat{F}_i\left(\boldsymbol{X}_{i,t}\right) + \widehat{G}_i\left(\boldsymbol{E}_{i,t}\right)$, where $\widehat{G}_i$ is also computed leaving out the $(i,t)^{th}$ point.

Not knowing the functional forms of our model a priori, we estimated the nonlinear functions F_i and G_i using hierarchical Bayesian Gaussian process (GP) regression as implemented in the GPEDM package (43). The hierarchical structure allows for heterogeneity in these functions across populations. To prevent overfitting, we set a prior with a mode of 0 on the importance of all lag predictors so that those which do not improve fit are effectively omitted (44, 45); see *SI Appendix*, Appendix B for more details on our hierarchical GP approach.

Model Selection and Analysis. We evaluated model performance using leave-one-out (LOO) out-of-sample $R^2 = 1 - \Sigma\left(x_{i,t} - \widehat{x}_{i,t}\right)^2 / \Sigma\left(x_{i,t} - \overline{x}_{i,t}\right)^2$. For each species, we fit models with the number of lags L ranging from 1 to 6 and selected the model with the L value that produced the highest R^2. In cases where a lower L produced a similar R^2_L [i.e., $R^2_L > 0.9 \times \max_d(R^2_d)$, $d \in 1{:}L$], we selected the more parsimonious model. More details on model selection, including selection of environmental drivers, is provided in *SI Appendix*, Appendix C.

To quantify the strength of environmental gradients relevant to a given species (Figs. 4*C* and 5 *C* and *D*), we first scaled each driver to the interval (0,1) across all populations and calculated the mean (across time) of each retained driver p and each population i, $\overline{E^p_i}$. We then calculated gradient magnitude $M^p = (\max_i \overline{E^p_i} - \min_i \overline{E^p_i}) / D$, where D is the maximum distance between populations for the species, and averaged M^p across all drivers. Finally, we analyzed the relation between average M and observed synchrony across species (Fig. 4*C*) by fitting a spline in mgcv and analyzing its slope using tsgam packages (46).

Throughout, we quantified synchrony as the expected Pearson correlation in log density between populations 350 km apart. This corrects for substantial variation in the geographic range of modeled species after data filtering (350 to 1,700 km). We chose 350 km because the metapopulations we modeled exceeded this distance in all but one species. We estimated synchrony using the ncf package (47), which fits a spline to the pairwise correlation between populations as a function of distance and then evaluated the spline at 350 km. To robustly evaluate predicted synchrony in models, we ran 1,000 simulations from each fitted EDM using permutations of the observed ("historical") environmental conditions (Figs. 4 *A* and *C* and 5). For each year and species, we set environmental values (or global mean-centered environmental values, for models without gradients) equal to those observed in a randomly selected year. We then simulate abundance by iterating the model year-by-year, using abundance predicted for one year to predict abundance in the following L years and measure synchrony in these simulations. In *SI Appendix*, Appendix D, we show that accounting for temporal autocorrelation in the environment had little impact on all our results.

Simulating Climate Change. Expected climatic changes in our study systems include increased variability in ocean climate indices ENSO (20), NPGO (48), NAO (29), an associated increase in heat wave frequency (28, 29), and increased mean temperature (2 to 5 °C by 2,100; ref. 49). Ongoing declines in latitudinal temperature gradients are also expected to continue (18), and the productivity gradient on the NE Shelf (Fig. 2*A*) is expected to flatten as zooplankton biomass declines disproportionately in the Gulf of Maine (24, 30). To explore the strategic implications of these changes for metapopulation synchrony, we first calculated the mean of each environmental driver p in each population i under historic conditions, $\overline{E^p_i}$, and deviations from these means, $E^{p*}_{i,t} = E^p_{i,t} - \overline{E^p_i}$. Next, we generated a set of 1,000-y permuted "historical" conditions as described above and randomly chose 40% of years to contain extreme events. In an extreme year, for each driver, we randomly choose a single value $\tilde{E^p}$ from the upper 25% or lower 25% of all values $E^{p}_{i,t}{}^*$. We then set $E^{p}_{i,t}$ in all locations to $\tilde{E^p} + \overline{E^p}_i$ in simulations with gradients present and to $\tilde{E^p}$ in simulations with gradients absent. Altogether, our approach simulates an increase in both the frequency and spatial extent of extreme events. For summer and winter temperatures, we sample extreme values only from the upper 10% of observations to simulate a conservative level of warming (NE Shelf: +2.3 °C; CA Current: +1.5 °C). We simulated models as described above.

Data, Materials, and Software Availability. Previously published data were used for this work (refs. 1–3, 5, 7–10, and 12 and reference 19 of the *SI Appendix*).

ACKNOWLEDGMENTS. V.A.K. was supported by NSF-OCE grant 2205794. D.C.R. was partly supported by US NSF grants 1714195 and 2023474, the James S. McDonnell Foundation, and the Alexander von Humboldt Foundation. We thank Mercedes Pozo, Nate Mantua, Andrew Thompson, and Tom Bell for data and helpful discussions on ocean climate change. Blue crab data for Virginia were provided by the Virginia Institute of Marine Science and for New Jersey by Rutgers University.

Author affiliations: [a]Department of Biology, University of Maryland, College Park, MD 20742; [b]Department of Ecology and Evolutionary Biology, University of Kansas, Lawrence, KS 66045; [c]Center for Ecological Research, University of Kansas, Lawrence, KS 66045; [d]Southwest Fisheries Science Center, National Marine Fisheries Service, National Oceanic and Atmospheric Administration, Santa Cruz, CA 95060; and [e]Department of Applied Mathematics, University of California, Santa Cruz, CA 95064

Author contributions: V.A.K. and S.B.M. designed research; V.A.K. performed research; S.B.M. and T.L.R. contributed new reagents/analytic tools; V.A.K. analyzed data; and V.A.K., S.B.M., T.L.R., and D.C.R. wrote the paper.

The authors declare no competing interest.

1. A. M. Liebhold, D. M. Johnson, O. N. Bjørnstad, Geographic variation in density-dependent dynamics impacts the synchronizing effect of dispersal and regional stochasticity. *Popul. Ecol.* **48**, 131–138 (2006).
2. O. N. Bjørnstad, R. A. Ims, X. Lambin, Spatial population dynamics: Analyzing patterns and processes of population synchrony. *Trends Ecol. Evol.* **14**, 427–432 (1999).
3. B. Grenfell *et al.*, Noise and determinism in synchronized sheep dynamics. *Nature* **394**, 674–677 (1998).
4. L. W. Sheppard, J. R. Bell, R. Harrington, D. C. Reuman, Changes in large-scale climate alter spatial synchrony of aphid pests. *Nat. Clim. Chang.* **6**, 610–613 (2016).
5. E. J. Defriez, D. C. Reuman, A global geography of synchrony for terrestrial vegetation. *Glob. Ecol. Biogeogr.* **26**, 878–888 (2017).
6. M. C. Castorani *et al.*, Disturbance and nutrients synchronise kelp forests across scales through interacting Moran effects. *Ecol. Lett.* **25**, 1854–1868 (2022).
7. B. B. Hansen, V. Grøtan, I. Herfindal, A. M. Lee, The Moran effect revisited: Spatial population synchrony under global warming. *Ecography* **43**, 1591–1602 (2020).
8. E. Palmqvist, P. Lundberg, Population extinctions in correlated environments. *Oikos* **83**, 359–367 (1998).
9. D. E. Schindler *et al.*, Population diversity and the portfolio effect in an exploited species. *Nature* **465**, 609–612 (2010).
10. K. C. Abbott, A dispersal-induced paradox: Synchrony and stability in stochastic metapopulations. *Ecol. Lett.* **14**, 1158–1169 (2011).
11. W. D. Koenig, Spatial autocorrelation and local disappearances in wintering North American birds. *Ecology* **82**, 2636–2644 (2001).
12. M. Peltonen, A. M. Liebhold, O. N. Bjørnstad, D. W. Williams, Spatial synchrony in forest insect outbreaks: Roles of regional stochasticity and dispersal. *Ecology* **83**, 3120–3129 (2002).
13. T. L. Rogers, S. B. Munch, Hidden similarities in the dynamics of a weakly synchronous marine metapopulation. *Proc. Natl. Acad. Sci. U.S.A.* **117**, 479–485 (2020).
14. S. B. Munch, S. Salinas, Latitudinal variation in lifespan within species is explained by the metabolic theory of ecology. *Proc. Natl. Acad. Sci. U.S.A.* **106**, 13860–13864 (2009).
15. D. O. Conover, T. M. Present, Countergradient variation in growth rate: Compensation for length of the growing season among Atlantic silversides from different latitudes. *Oecologia* **83**, 316–324 (1990).
16. S. B. Munch, M. Mangel, D. O. Conover, Quantifying natural selection on body size from field data: Winter mortality in Menidia menidia. *Ecology* **84**, 2168–2177 (2003).
17. B. J. Sinclair, C. M. Williams, J. S. Terblanche, Variation in thermal performance among insect populations. *Physiol. Biochem. Zool.* **85**, 594–606 (2012).
18. H. Baumann, O. Doherty, Decadal changes in the world's coastal latitudinal temperature gradients. *PLoS One* **8**, e67596 (2013).
19. N. Pepin *et al.*, Elevation-dependent warming in mountain regions of the world. *Nat. Clim. Chang.* **5**, 424–430 (2015).
20. W. Cai *et al.*, Increasing frequency of extreme El Niño events due to greenhouse warming. *Nat. Clim. Chang.* **4**, 111–116 (2014).
21. G. J. Di Cecco, T. C. Gouhier, Increased spatial and temporal autocorrelation of temperature under climate change. *Sci. Rep.* **8**, 14850 (2018).
22. E. C. Oliver *et al.*, Projected marine heatwaves in the 21st century and the potential for ecological impact. *Front. Mar. Sci.* **6**, 734 (2019).
23. B. Hugueny, Spatial synchrony in population fluctuations: Extending the Moran theorem to cope with spatially heterogeneous dynamics. *Oikos* **115**, 3–14 (2006).
24. A. J. Pershing *et al.*, Climate impacts on the Gulf of Maine ecosystem: A review of observed and expected changes in 2050 from rising temperatures. *Elementa Sci. Anthrop.* **9**, 00076 (2021).
25. E. Perez *et al.*, Understanding physical drivers of the 2015/16 marine heatwaves in the Northwest Atlantic. *Sci. Rep.* **11**, 17623 (2021).
26. K. Sherman, J. Kane, S. Murawski, W. Overholtz, A. Solow, "6 The US Northeast shelf large marine ecosystem: Zooplankton trends in fish biomass recovery" in *Large Marine Ecosystems* (Elsevier, 2002), pp. 195–215.
27. M. L. Pinsky, B. Worm, M. J. Fogarty, J. L. Sarmiento, S. A. Levin, Marine taxa track local climate velocities. *Science* **341**, 1239–1242 (2013).
28. F. P. Chavez *et al.*, Readying California fisheries for climate change (2017).
29. S. M. Vicente-Serrano *et al.*, Extreme winter precipitation in the Iberian Peninsula in 2010: Anomalies, driving mechanisms and future projections. *Clim. Res.* **46**, 51–65 (2011).
30. B. D. Grieve, J. A. Hare, V. S. Saba, Projecting the effects of climate change on Calanus finmarchicus distribution within the US Northeast Continental Shelf. *Sci. Rep.* **7**, 1–12 (2017).
31. C. Cai, Y.-O. Kwon, Z. Chen, P. Fratantoni, Mixed layer depth climatology over the northeast US continental shelf (1993–2018). *Cont. Shelf Res.* **231**, 104611 (2021).
32. S. B. Hagen, J. U. Jepsen, N. G. Yoccoz, R. A. Ims, Anisotropic patterned population synchrony in climatic gradients indicates nonlinear climatic forcing. *Proc. R. Soc. B Biol. Sci.* **275**, 1509–1515 (2008).
33. S. Engen, R. Lande, B.-E. Sæther, T. Bregnballe, Estimating the pattern of synchrony in fluctuating populations. *J. Anim. Ecol.* **4**, 601–611 (2005).
34. B.-E. Sæther *et al.*, The extended Moran effect and large-scale synchronous fluctuations in the size of great tit and blue tit populations. *J. Anim. Ecol.* **76**, 315–325 (2007).
35. A. L. Fredston *et al.*, Marine heatwaves are not a dominant driver of change in demersal fishes. *Nature* **621**, 324–329 (2023).
36. D. Esguerra, S. B. Munch, Accounting for observation noise in equation-free forecasting: The hidden-Markov S-map. *Methods Ecol. Evol.* **15**, 1347–1359 (2024).
37. B. Johnson, M. Gomez, S. B. Munch, Leveraging spatial information to forecast nonlinear ecological dynamics. *Methods Ecol. Evol.* **12**, 266–279 (2021).
38. C. T. Perretti, S. B. Munch, G. Sugihara, Model-free forecasting outperforms the correct mechanistic model for simulated and experimental data. *Proc. Natl. Acad. Sci. U.S.A.* **110**, 5253–5257 (2013).
39. G. Sugihara *et al.*, Detecting causality in complex ecosystems. *Science* **338**, 496–500 (2012).
40. V. Poynor, S. Munch, Combining functional data with hierarchical Gaussian process models. *Envir. Ecol. Stat.* **24**, 175–199 (2017).
41. F. Takens, "Detecting strange attractors in turbulence" in *Dynamical Systems and Turbulence*, D. A. Rand, L. S. Young, Eds. (Elsevier, 1981), pp. 366–381.
42. J. Stark, Delay embeddings for forced systems. I. Deterministic forcing. *J. Nonlin. Sci.* **9**, 255–332 (1999).
43. S. B. Munch, T. L. Rogers, GPEDM: Gaussian Process regression for Empirical Dynamic Modeling (R package version 0.0.0.9007, 2023). https://tanyalrogers.github.io/GPEDM. Accessed 13 December 2024.
44. J. Molofsky, Population dynamics and pattern formation in theoretical populations. *Ecology* **75**, 30–39 (1994).
45. E. Ranta, V. Kaitala, P. Lundberg, Population variability in space and time: The dynamics of synchronous population fluctuations. *Oikos* **83**, 376–382 (1998).
46. G. Simpson, tsgam: Utilities for Working with GAMs Fitted to Time Series (R package version 0.0-4, 2018). https://github.com/gavinsimpson/tsgam. Accessed 13 December 2024.
47. O. N. Bjørnstad, ncf: Spatial Covariance Functions (R package version 1.2-9, 2020). https://CRAN.R-project.org/package=ncf. Accessed 13 December 2024.
48. E. Di Lorenzo, N. Mantua, Multi-year persistence of the 2014/15 North Pacific marine heatwave. *Nat. Clim. Chang.* **6**, 1042–1047 (2016).
49. A. H. Khan, E. Levac, G. L. Chmura, Future sea surface temperatures in Large Marine Ecosystems of the Northwest Atlantic. *ICES J. Mar. Sci.* **70**, 915–921 (2013).